

Intercomparison of Inversion Algorithms for Particle-Sizing using Mie Scattering

Norbert Riefler^{†*} and Thomas Wriedt[‡]

March 10, 2008

[†]Universität Bremen, FB4, Verfahrenstechnik, Badgasteiner Strasse 3, 28359 Bremen, Germany

[‡]Stiftung Institut für Werkstofftechnik, Badgasteiner Strasse 3, 28359 Bremen, Germany

Keywords: Inverse problem, regularization methods, elliptical mirror

Abstract

We examine the applicability of different inversion algorithms to retrieve a size distribution of particles in air from light scattering. Our investigation is focused on an optical measurement setup with an elliptical mirror as the main optical element. To evaluate the capabilities of the individual inversion methods, we simulate light scattering by spherical particles in the size range of 0.1 - 10 μm and in the size range of 0.05 - 1 μm . The distribution of the particle diameters is modeled with three different parametric functions (RRSB, logarithmic-normal and a more special distribution from an ultrasonic nebulizer). Different kinds of noise (additive and/or multiplicative) in different levels are applied to the simulated scattering measurement to include real physical measurement conditions. We investigate the convergence properties of the scattering simulation with respect of the number of size classes and in this way get information about the necessary size resolution to simulate a measurement for a given particle size distribution. Further parameters of interest are the minimum angular resolution of the measurements, the number of size classes of the retrieved particle size distribution and the measured polarization of the scattered light.

1 Introduction

Optical particle characterization is needed in many practical applications as, for example, for aerosol analysis, investigation of air pollution, weather radar problems, remote sensing, etc. The size distribution of small particles is frequently measured by evaluating the light scattering response of an incident laser beam. In many of those measuring applications there are more than a single particle within the measurement volume. For the characterization of a particle size distribution, a frequently used method is laser diffraction [1]. Information about the particles is gathered by evaluation of the scattered light. If the particles are distributed randomly and their optical density can be assumed to be small, then the scattered intensity $I(\theta)$ at scattering angle θ is an incoherent superposition of the scattering pattern I_n of all N particles ($n = 1, \dots, N$) within the measuring volume. This assumption is only an approximation for real physical systems because of mutual interaction caused by multiple scattering of the particles due to their finite distances, and additionally because of noise due to the measurement electronics. Therefore, noise will be added to a model system (i.e. to the scattered intensities) to include the unknown physical conditions of the measurement system.

A vast number of publications deal with one or more methods to solve the inverse problem of a particular application of a measuring system. Most of the papers describe new inversion algorithms and they sometimes compare the results with those from well-known standard methods. In the following, we only want to cite some important major papers to give an overview.

An overview of general inverse problems are given in the textbooks of Hansen [2], Ramm [3], Tarantola [4] and in the monograph of Gosh Roy and Couchman [5] for the case

*To whom correspondence should be addressed (riefler@iwt.uni-bremen.de)

of incident plane waves. For analysing aerosol measurements a review is given in the paper by Kandlikar and Ramachandran [6].

In a recently published paper, Vargas-Ubera et al. [7] compare three inversion methods, the Chin-Shifrin [8], Phillips-Twomey [9] and singular value decomposition method on the basis of Fraunhofer approximation and calculations of the light scattering using Mie theory. Simulating this inversion problem, they found that the Phillips-Twomey method yields the best, the singular value decomposition only delivers satisfactory and the Chin-Shifrin method yields poor results. However, the Chin-Shifrin method provides an exact analytical solution of the inverse problem (eq (1)) by using Fraunhofer approximation for the scattering intensities, and it was proposed to use in particle sizer by Bayvel and co-workers [10]. The same author published another paper where he and his co-authors recommend the use of the Phillips-Twomey method for the particle size retrieval [11]. In fact, the Phillips-Twomey method was investigated already by Chow and Tien [12] and is nowadays a standard method in inverse problems in particular of laser diffraction measurements and is used by many workers (e.g. [13, 14]).

Another method is to replace the particle size distribution by a spline approximation and then to apply a regularization technique [15]. Sun and Sevick-Muraca [16] describe a B-spline approximation method with a subsequent Tikhonov regularization with the generalized cross validation or the L-curve method to estimate the regularization parameters.

Iterative methods used to retrieve data from light scattering measurements include for instance Chahine iteration, Landweber iteration, evolutionary algorithms like genetic algorithms and neural networks. Chahine developed his algorithm on the basis of problems in the radiative transfer of the atmosphere [17], but it is also used to analyze fractals [18] or for the size characterization of inhomogeneous droplets by phase Doppler anemometry [19]. Landwebers' algorithm [20] can also be used for different kinds of problems like image-reconstruction [21] or particle sizing [19].

In contrast to both methods, the evolutionary approaches are more complex. Genetic algorithms for instance are considered slow, but they yield stable solutions [22, 23].

The last class of iterative methods are the neural networks, which do not optimize a solution on a given pattern, instead they are used to find patterns in data by a previously trained model. Applications to light scattering problems are given by Nascimento et al. [24], Wang et al. [25] and Coppens et al. [26].

Measurement of additional physical properties of the scattered light, e.g. polarization, range of scattering angles, is important for the retrieval of particle size distributions. In most of the mentioned papers light scattered in forward direction is evaluated, while Barkey et al. [23], Hodgson et al. [22], Wang et al. [25] and Ho et al. [27] have presented results using complete scattering diagrams. However, they investigate only particles with a Mie parameter $\alpha < 10$. The scattering diagrams are evaluated by using only one polarization [22, 25], using horizontal and vertical polarization [23] or using the Mueller matrix formalism [27], which delivers the most information regarding polarization.

In this paper, we will apply more than 20 different inversion methods to a simulated scattering pattern of a given particle size distribution corresponding to a particular measurement setup. This serves as an overview of the applicability of different methods to our measurement setup. Several of the used inverse problem methods are based on SVD, e.g. truncated and damped SVD together with different regularization approaches like Tikhonov regularization [2]. Other methods are based on the non negative least square approach in combination with Philips-Twomey regularization [9, 13, 14]. Iterative approaches like those of Chahine or Landweber and Bialy are described by Chahine [17] and by Mitschke [19], respectively. Other iterative methods of interest are the genetic algorithm approach [22, 28] and an inverse Monte Carlo technique [29].

The first aim of this paper is to investigate the effects on the inversion methods when using different simulation techniques to prepare the data. For instance, the matrix elements of the kernel matrix h in the inversion formula can consist on normalized or not normalized scattering diagrams. Another effect appears in the simulation of a measurement. To simulate the measurement of the light scattering of a continuous particle size distribution the number of the used particles with different diameters is crucial for convergence.

The second aim of this paper is to find the best inversion method for a particular measurement setup using an elliptical mirror, represented in Figure 1. The advantage of an elliptical mirror is that the scattered light can be measured simultaneous in contrast to

e.g. a goniometric setup. Additionally, a setup like that of Figure 1 permits the acquisition of a nearly complete scattering diagram of about $5^\circ \leq \theta \leq 175^\circ$ on the left and the right semicircle of the mirror.

In general, the angular resolution of a measurement combined with the number of different measuring points is also important for the determination of the correct PSD [1]. A higher resolution seems to be better as long as noise, always omnipresent in measurement systems, does not decrease below a reasonable value. This requires the investigation of the effects of noise, what has also been done e.g. by Coston and George [30]. Here, we distinguish between additive and multiplicative noise (“speckle noise” and “shot noise” in [30]). As it is not clear how the investigated inversion methods respond to these noise formulations, these effects will be investigated also in the following as our third aim.

This paper is divided as follows. In the next section we describe our approach to simulate experimental measurements and the generation of the kernel matrix h . Then, we give a short presentation of the inversion methods used. The results are listed and discussed in the following section. Finally, we sum up our findings with a conclusion.

2 Inversion Problem

Elliptical mirrors are occasionally used as the main optical element in light scattering experiments. For instance, a description of an single-particle optical counter using an ellipsoidal mirror is given by Friedlander [31]. Aptowicz and Chang [32] also describe a measurement system with an ellipsoidal mirror to investigate different single particles as well as particle clusters. They use a two-dimensional analysis of the picture taken by an intensified CCD-camera, but without any inversion method. We want to investigate a measurement setup for particles in air given in Figure 1. The scattered light of an almost complete scattering plane can be focused on a CCD-camera. Alternatively, the horizontal polarized scattered light is measured at one side (e.g. the left semicircle in respect of the incident beam) of the mirror whereas the vertical polarization is measured at the other side (e.g. the right semicircle). In the following, we treat the investigated inversion algorithms with respect to the geometry of an ellipsoidal mirror.

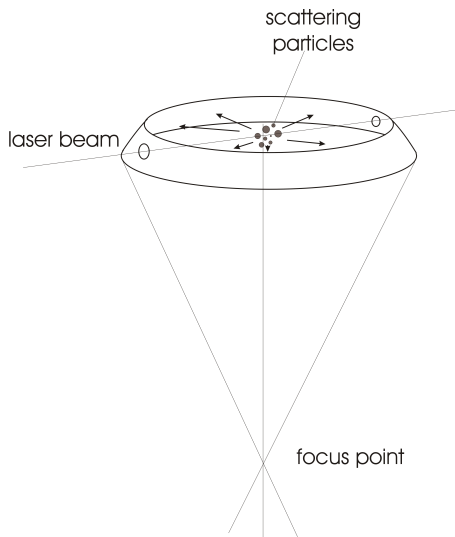


Figure 1: Investigated experimental setup; a laser beam illuminates particles at the first focal point of an ellipsoidal mirror; the light scattered from the particles will be mapped onto the second focal point and from there the light will be collected with a lens to form a – nearly – circular image of the scattered light from the mirror on a CCD camera.

Generally, the measured intensity $I(\theta, \lambda)$ depends on the laser wavelength λ , the physical properties of the particles (diameter x and the refractive index $m = n - i\kappa$ relative to the surrounding medium) and the particle size distribution (PSD) $q(x)$:

$$I(\theta, \lambda) = \int_0^\infty I_n(\theta, \lambda, m(\lambda), x)q(x)dx. \quad (1)$$

If the particles consist of a homogeneous material and they are illuminated by monochromatic light, this equation corresponds to a Fredholm integral equation of the first kind [2] with minimum and maximum diameter x_{min} and x_{max} :

$$g(\theta) = \int_{x_{min}}^{x_{max}} h(\theta, x)q(x)dx \quad (2)$$

where $g(\theta)$ corresponds to a measured value, $h(\theta, x)$ is an element of the given kernel \mathbf{H} which consists of simulated Mie scattering diagrams, and $q(x)$ is the unknown PSD. To get an impression of such a kernel, Arridge et al. [33] represented an isometric plot of a kernel consisting of scattering diagrams for spheres with Mie parameter $\alpha = \pi d/\lambda$ between 0 and 50. To resolve the continuous size distribution $q(x)$, equation (2) reads in its discrete form [5]:

$$\mathbf{g} = \mathbf{H}\Delta\mathbf{Q}, \quad (3)$$

with \mathbf{g} as the vector of all measured values $g(\theta)$ at different scattering angles θ and $\Delta\mathbf{Q} = [\Delta Q(x_1), \dots, \Delta Q(x_n)]^T$ represents the frequency distribution which is related to the particle size distribution by the frequency width Δx , $\Delta\mathbf{Q} = \mathbf{q} \cdot \Delta\mathbf{x}$. The kernel matrix \mathbf{H} consists of the matrix elements $h(\theta, x)$. Equation (3) is a forward problem and the expected measurement values $g(\theta)$ can be easily determined by calculation of the the matrix elements of $h(\theta, x)$ using Mie theory for a particle size distribution $q(x)$. However, the determination of the particle size distribution from measurement data \mathbf{g} is an inverse problem:

$$\Delta\mathbf{Q} = \mathbf{H}^{-1}\mathbf{g}. \quad (4)$$

A direct evaluation is impossible. Inverse problems are typically ill-posed. The solution of a well-posed problem has to fulfill the conditions of existence, uniqueness and stability. Especially in inverse problems, the condition of stability is violated due to measuring noise. Additionally, inverse problems are mostly ill conditioned. A measure of the ill conditioning of the problem is the condition number κ of the kernel matrix \mathbf{H} , $\kappa = \|\mathbf{H}\| \|\mathbf{H}^{-1}\|$. $\kappa \ll 1$ implies a high degree of ill-conditioning due to, e.g. simple rounding errors. Hence, simple matrix inversion methods like the LU-decomposition are unsuitable solution methods for an inverse problem. Mathematically more complex methods have to be used to yield useful results. The methods can be classified by the following schemes [5]:

1. evaluation of spectral properties of the normal operators after a singular value decomposition (SVD) of the kernel matrix h and application of filtering methods
2. transforming an ill-posed problem into a well-posed one by regularization
3. iterative approaches.

These three schemes can be combined to get new methods [19]. There are further schemes to tackle inverse problems, e.g. mollification methods or pure least square optimization, but we will not discuss them here. All schemes own the positivity constraint, that no negative diameters are possible.

The intention of our paper is to find inversion methods which are suitable to approximate a given particle size distribution with well known refractive index from light scattering measurements without any a priori assumptions. For example, we do not assume that a given particle size distribution will represent our measurements and therefore we do not fit two or three distribution parameters to the given measurements. From the great number of inversion methods we selected some major methods for our investigations.

We investigate small droplets with diameters up to 10 μm . The droplet deformation can be calculated by $D = (19\lambda + 16)Ca / (16\lambda + 16)$ (with $Ca = \eta v / \sigma$ as the capillary number (viscosity η , surface tension σ) and λ the viscosity ratio droplet/gas) [34]. This equation lead to drop deformations of up to 8% for particle velocities of $v = 5$ m/s. However, the equation do not take into account the size of the droplets. For the investigated small droplets, the Weber number is much less than 1 and therefore the droplet deformation can be neglected [35].

3 Numerical Experiments

To test the suitability of different inversion algorithms, we simulate light scattering of spherical water droplets with a well known refractive index ($n=1.33$) in the size range of $d = 0.1 - 10\mu m$ and of $d = 0.05 - 1\mu m$ at a typical laser wavelength of $\lambda = 514.5nm$. This means, the maximum of the dimensionless Mie parameter is $\alpha = \pi d/\lambda = 61$. In real processes, the particle diameters are statistically distributed and this will be described in this paper using three different particle size distributions (PSD) $q(x)$ [1]. In principle, these size distributions correspond to probability density functions. The well-known log-normal distribution function has the form:

$$q(x) = \frac{1}{\sqrt{2\pi x\sigma}} \exp\left(-\frac{(\ln(x) + \ln(\bar{d}))^2}{2\sigma^2}\right) \quad (5)$$

with the standard deviation σ and the arithmetic mean value of the diameter \bar{d} . An example (light blue solid line) can be viewed in figure 2.

An often used drop size distribution function common to spray processes is the RRSB (Rosin-Rammler-Sperling-Bennet) distribution function [36]:

$$Q(x) = 1 - \exp\left(-\left(\frac{x}{\bar{d}}\right)^n\right). \quad (6)$$

The shape of this distribution function are determined by the mean diameter \bar{d} and n , which determines the width of the distribution. A value of $n > 2$ belongs to a nearly monodisperse distribution. To get the probability density, i.e. the PSD, one have to differentiate $Q(x)$, $q(x) = dQ(x)/dx$ (e.g. the dark blue dashed-dotted line in figure 2).

A third distribution function is taken from an investigation of ultrasonically produced water droplets described by Hedrih et al. [37]:

$$q(x) = \frac{128}{3\bar{d}^4} \cdot x^3 \exp\left(-4\frac{x}{\bar{d}}\right). \quad (7)$$

Again, an example is given in Figure 2 (red dashed line). Ultrasonic nebulizers are used to produce broad size distributions [38] to test measuring devices.

Each of these three PSDs are used to simulate the scattering response of hypothetical measurements. They represent different broad PSDs, shown in Figure 2 with the corresponding parameters. Of course, one can also get PSDs with differing widths from the log.-normal or the RRSB distribution, and we present as well results of a varied log.-normal PSD and a bimodal PSD in section 5.

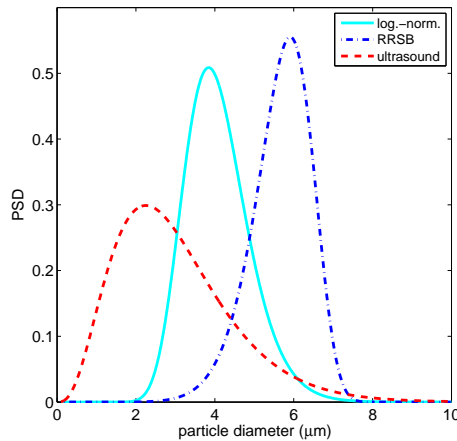


Figure 2: Normalized log-normal ($\bar{d} = 4.08\mu m$, $\sigma = 0.2$, $d_{50} = 3.98\mu m$), RRSB ($\bar{d} \approx d_{50} = 4.57\mu m$, $n = 9$, $d_{63} = 4.94\mu m$) and ultrasonic PSD ($\bar{d} = 2.99\mu m$, $d_{mod} = 2.24\mu m$, $d_{63} = 3.23\mu m$)

3.1 Simulation of Measurements

We want to describe the effects of the number of different size values x_i (i is the number of a node) used for integration in eq. (1) and (2) as well as the effect of low resolutions in the scattering angles. This is an important topic because for testing and evaluating different inversion methods it seems to be necessary to simulate measurements which take into account realistic ambient conditions as far as possible. Therefore, we have to investigate how to generate a simulated measurement on the basis of simulated scattering patterns, i.e. how many scattering patterns have to be used to give a convergent result, and in which way noise has to be added to achieve a realistic measured signal.

The consideration of convergent scattering diagrams does not take into account the real number of droplets in a measurement volume. If we assume a measurement volume of $V = 1 \text{ mm}^3$ and use a criterion for the maximum volume concentration c_V at which the light scattering process fulfills the single scattering requirement, $c_V \leq 0.01$ [39, 31], there are several thousands droplets with diameter $x = 10 \mu\text{m}$ for $c_V = 0.01$ and even some millions when $x = 1 \mu\text{m}$ within the measurement volume. Therefore we use convergent scattering diagrams which consist of several hundred different diameters (i.e. nodes). However, we also simulate measurements of the light scattering with randomly choosen particle diameters according to a probability which is related to the PSD.

In order to check the used computer programs for correct results, we compare the scattering diagrams of algorithms by Wiscombe [40] and an implementation of the code by Bohren and Huffman [38]. There are no numerical differences within the considered range of particle sizes used in the present study, so each program can be used. Most of the time, the code of Bohren and Huffman is employed.

The simulation of a measured scattering response requires an assumption about the number of particles n_{part} within the measurement volume. The particle sizes are statistically distributed according to the supposed PSD. Then, the scattering response will be determined by the superposition – i.e. an addition – of the scattering diagrams of each particle.

Because of the unknown, arbitrary choosen number of particles within a measurement volume, we simulate additionally convergent scattering measurements. Convergence is reached when the simulated resulting scattering diagram do not change with an increasing number of nodes n_{node} of different size values x_i . In general, the more nodes are used, the smoother will be the numerical integration of eq. (1) and (2). For instance, a simulated measurement using a small number of nodes of $n_{node} = 20$ differs considerable from that using a number of nodes of $n_{node} = 100$, see Figure 3. However, $n_{node} = 500$ is sufficient for a convergent scattering diagram in this particular case of horizontal-horizontal- (hh-) and vertical-vertical- (vv-) polarization, I_{hh} and I_{vv} . When using unpolarized light (i.e. the intensity is a summation of I_{hh} and I_{vv} , $I_{unpol} = (I_{hh} + I_{vv})/2$), the number of nodes should be increased to at least $n_{node} = 1000$. For this, one gets the simulated scattered diagrams for the three described PSDs from above, represented in Figure 4. The results show that two PSDs with similar width but different mean diameter (log. normal and RRSB distribution) result in obviously different scattering diagrams. However, although their mean diameters are different, the scattering diagram of the broader ultrasonic distribution looks very similar to that of the log. normal distribution. The differences between the scattering patterns of the RRSB distribution from the other patterns might be explained by the strong increase of the number of oscillations in a scattering diagram with increasing particle diameter. The ultrasonic and the log. normal distribution, on the other side, reveal very similar scattering diagrams because their mean diameter is comparatively small. An enlarged detail of the forward scattering range of Figure 4 (right part) shows three disinct diagrams. As a consequence it can be assumed that the PSDs with small particles ($\alpha < 5$) will give flat scattering curves without oscillations.

A minor effect on the convergence of the scattering diagram is given by the variation of the resolution of the scattering angle θ for the calculated diagrams. A high resolution of $\Delta\theta = 0.1^\circ$ did not show any differences regarding a complete scattering diagram compared to that with $\Delta\theta = 1^\circ$ in respect of the convergence behaviour. However, sharp minima within the diagrams are resolved only for an angular resolution of at least $\Delta\theta = 0.25^\circ$.

Above all, we also have to include noise into the simulated measurements due to the ambient physical conditions (e.g. unwanted scattered light from reflections), due to noise in the measurement electronics, and due to multiple scattering effects between the particles because of the coherent laser light [41]. The level of the noise has an influence on the

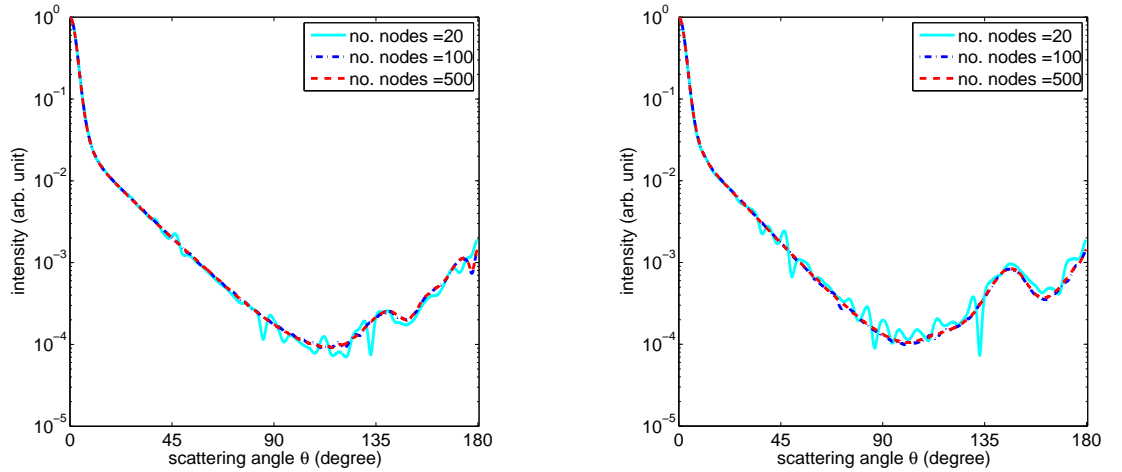


Figure 3: Convergence of scattering diagrams for different node numbers with respect to horizontal-horizontal (left) and vertical-vertical (right) polarized laser light (wavelength $\lambda = 514.5nm$) using the ultrasonic PSD for water particles ($n = 1.33$) represented in Figure 2

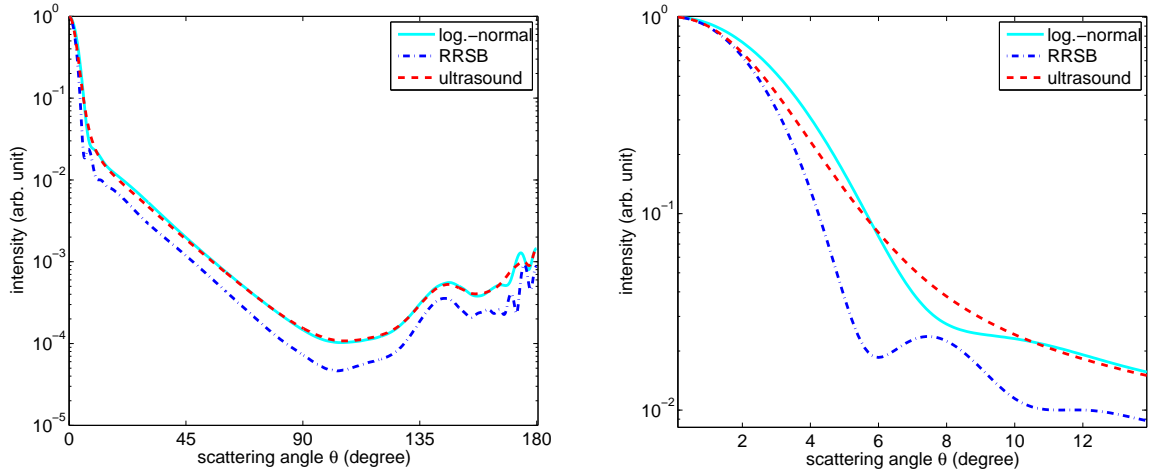


Figure 4: Left: scattering diagrams for three different PSDs of Figure 2 using a number of nodes of 1000 and unpolarized light; right: detailed enlargement of the forward scattering range from Figure 4

regularization parameters of the inversion algorithms [3]. Therefore, we add noise to the simulated measurements in different levels. In general, there are multiplicative (γ) and additive (ϵ) noise which disturbs a signal. Multiplicative noise due to multiple scattering can be related to speckle phenomena [42, 43] as well as to fading in communication systems [44, 45], while additive noise is a rather general phenomena which occurs, e.g. in the resistor noise of electronic circuits or in CCD-cameras as well as from the unwanted detection of light from arbitrary sources.

Because the nature of multiplicative noise is usually the superposition of coherent waves, even the forward scattering intensities are influenced by that kind of noise. On the other hand, additive noise originates from attenuation and distortion of the measured signals [46]. The effect of both kinds of noise on a measured scattering diagram can be expressed by:

$$g_{\epsilon,\gamma}(\theta) = g(\theta)\gamma + \epsilon. \quad (8)$$

In this paper we will account for the multiplicative noise mainly to the previously integrated scattering response of the particle collective. Additionally, we apply this kind of noise to the scattering diagrams of each particle. The multiplicative noise parameter γ is determined

by [47, 48, 23]:

$$\gamma = (1 - p/2) + pX, \quad (9)$$

with $X \in [0, 1]$ as a white Gaussian process generated by a Gaussian random number generator and p as the noise factor. $p = 0.1$ means that the signal will be degraded by a noise level of 10%. In the case of additive noise we use the usual signal-to-noise ratio (SNR), e.g. defined by [49]: $SNR = 10 \log(\sigma_g/\sigma_N)$ with σ_g, σ_N as the variance of the signals g and N to characterize the magnitude of the additive noise. ϵ is also determined by a white Gaussian process, and the maximum values of ϵ are limited by the given SNR. Therefore, this additive noise floor affects in particular weak signals like the intensity of particles at scattering angles about $\theta = 90^\circ$, while the strong forward scattering will be barely affected.

3.2 Kernel Matrix Generation

After we have given some general consideration about the generation of a simulated measurement, we will now describe some consequences on the inversion algorithms when parameters of the kernel matrix will be varied.

The matrix elements of each row of the kernel \mathbf{H} (eq. (3)) consist on calculated scattering intensities at all measured scattering angles depending on the size class x_i . Therefore, it is possible to normalize the kernel matrix elements to a previously specified value of one matrix element. In the results presented in this paper, we normalize to the first measured scattering angle which is set to a value of 1.

On the other hand, the kernel matrix can be built by the raw scattering diagrams from the simulation program. The differences of the intensity values between particles with diameter of $x = 0.1\mu m$ and $10\mu m$ is very high, in the order of magnitude of about 10^6 . Nevertheless, there are some inversion algorithms which deliver correct or at least much better results when the kernel do not consist of scaled scattering diagrams, whereas some other algorithms work only if the scattered diagrams of the kernel are normalized. Therefore, it seems to be of interest to investigate which inversion algorithm works best with a scaled kernel and which with an unscaled one.

Another import parameter is the number of size classes, n_i . A too large number can often lead to oscillations in the resulting PSD curve, while a too small number cannot reproduce the PSD in sufficient resolution. The discretization of the PSD is accomplished without interpolation. Reasonable values are $n_i \approx 20 \dots 40$. Because of this we choose a number of $n_i = 24$ for most of the simulations. The division of the scale is linear, but we also present a geometric series division which may be advantageous for specific PSDs.

The retrieval of a PSD with a number of size classes n_i is related to number of measurements m , which is given by the length of $g(\theta)$. The condition to get a solution of the linear system in eqn. 4 is $m \geq n_i$. However, an increase of m will not necessarily lead to more stable or more accurate solutions because the eigenvalues of the covariance matrix $\mathbf{C} = \mathbf{H}_{m \times n_i} \mathbf{H}_{n_i \times m}^{-1}$ may become very small and therefore the information content tend to zero [9]. However, in some cases – although the eigenvalues are very small ($< 10^{-10}$) – an increase of the number of measurements is necessary for a correct retrieval of the PSD. We refer to this circumstance again below.

4 Inversion Methods

A detailed description of the used inversion methods would exceed the limit of this paper, so we only give a short sketch in the order of the methods listed in Table 1. The *singular value decomposition* (SVD) of a rectangular matrix \mathbf{H} is a decomposition:

$$\mathbf{H} = \mathbf{U} \mathbf{\Sigma} \mathbf{V}^T \quad (10)$$

with the diagonal matrix $\mathbf{\Sigma} = \text{diag}(\sigma_1, \dots, \sigma_n)$, which consists of non-negative singular values σ_i in decreasing order. $\mathbf{U} = (\mathbf{u}_1, \dots, \mathbf{u}_n)$ and $\mathbf{V} = (\mathbf{v}_1, \dots, \mathbf{v}_n)$ are orthonormal matrices ($\mathbf{U}^T \mathbf{U} = \mathbf{V}^T \mathbf{V} = \mathbf{I}$, \mathbf{I} as the identity matrix, T depicts the transpose). In the case of non-quadratic, rectangular matrix \mathbf{H} , the Generalised SVD is used, but the following description remains in principle the same.

abbrev.	algorithm	references
SVD	Singular-Value-Decomposition	Hansen [2]
TSVD	Truncated SVD	Hansen [2]
DSVD	Damped SVD	Hansen [2]
NNLS	Non-Negative Least Squares	Lawson, Hanson [50]
P.-T.	Phillips-Twomey	Weichert [14]
Tikh.	Tikhonov	Hansen [2]
GA	Genetic Algorithm	Hodgson [22]
L.-B.	Landweber-Bialy	Mitschke [19]
Chah.	Chahine	Mitschke [19]
IMC	Inverse Monte-Carlo	Ligon et al. [29]

Table 1: List of the methods used for comparison; some abbreviations label more than one algorithm (see the text).

Roughly speaking, the small singular values of the diagonal matrix Σ represent the noise of a system. The simple solution of eq. (3) by means of a SVD is to calculate the so-called pseudoinverse of \mathbf{H} by:

$$\mathbf{H}^{-1} = \mathbf{V}\Sigma^{-1}\mathbf{U}^* \quad (11)$$

with $\Sigma^{-1} = \text{diag}(1/\sigma_1, \dots, 1/\sigma_n)$ and \mathbf{U}^* as the complex conjugate of \mathbf{U} . However, this pseudoinverse rarely delivers useful or correct results. However, the SVD serves as a base for other methods like the truncated (TSVD) and the damped (DSVD) SVD. In the case of TSVD, a simple truncation of all small singular values σ_i , starting from an index n_t , and a following recalculation of \mathbf{H} results in an improved solution compared to the SVD, and frequently the TSVD delivers the only stable solution of equation 3. However, the problem is to find the best truncation number for the σ_i . For the TSVD, we use five different methods:

1. *TSVD LSQ optimized*: The least square differences of the known PSD and the solution $q_t = \mathbf{V}\Sigma_{n_t}^{-1}\mathbf{U}^T$ are calculated for each truncation number $n_t = 1, \dots, n$ to find the n_t with the best fit. Such an a priori calculated, constant truncation number may be sufficient to retrieve the PSD for a specific measurement problem.
2. *TSVD with L-curve*: This is a graphical method. A full-logarithmic plot of the residual norm $\|\mathbf{H}\mathbf{q} - \mathbf{g}\|$ versus the corresponding norm of different solutions for the PSD \mathbf{q} , $\|\mathbf{I}\mathbf{q}\|$, usually shows an extremal value, for which the corresponding truncation number n_t is the optimized solution.
3. *TSVD with Generalized Cross-Validation (GCV)*: Minimization of

$$G = \frac{\|\mathbf{H}\mathbf{q}_{reg} - \mathbf{g}\|^2}{n - \sum_{i=1}^p f_i}, \quad (12)$$

with $f_i = \sigma_i^2/(\sigma_i^2 + \lambda^2)$ as the (Wiener) filter factors, $p = 1, \dots, n - 1$ and $\mathbf{q}_{reg} = \sum_{i=1}^n f_i \mathbf{u}_i^T \mathbf{g} \mathbf{v}_i / \sigma_i$, gives the best, regularized solution \mathbf{q}_{reg} for the PSD.

4. *TSVD with Quasi Optimality Criterion (QOC)*: Minimizing of

$$Q = \left(\sum_{i=1}^p \left(f_i (1 - f_i) \frac{\mathbf{u}_i^T \mathbf{g}}{\sigma_i} \right)^2 \right)^{1/2} \quad (13)$$

with f_i as the (Wiener) filter factors and using different regularization parameters λ to filter out the noise in h .

5. *Modified TSVD (MTSVD) with L-curve*: Similar to the TSVD with L-curve above, but here using a concatenated vector \mathbf{q}_0 on \mathbf{q} which minimizes the norm $\|\mathbf{q}\|$.

Non Negative Least Square (NNLS) minimizes the norm $\|\mathbf{H}\mathbf{q} - \mathbf{g}\|$ with the condition $\mathbf{q} \geq 0$ for every element of \mathbf{q} . The NNLS will also be used by the following Phillips-Twomey (P.-T.) regularization methods:

1. *P.-T. with LSQ optimized regularization parameter λ* : This calculates the SVD of the matrix $\mathbf{H}^T\mathbf{H} + \lambda\mathbf{S}$ with the banded matrix [13]

$$\mathbf{S} = \begin{pmatrix} 0 & 0 & 0 & 0 & \cdots \\ -1 & 2 & -1 & 0 & \cdots \\ 0 & -1 & 2 & -1 & \cdots \\ \vdots & \vdots & \vdots & \vdots & \ddots \end{pmatrix}. \quad (14)$$

2. *P.-T. with NNLS*: This method uses a predefined regularization parameter λ to calculate a regularization matrix $\mathbf{H}^{reg} = \mathbf{H}^T\mathbf{H} + \lambda\mathbf{S}$ and then minimization of $\|\mathbf{H}^{reg}\mathbf{q} - \mathbf{g}\|$ using NNLS.

In the Tikhonov regularization (Tikh.) four different methods are used to find an optimized solution:

1. *Tikh. with L-curve*: Minimization of the combined norm of $\|\mathbf{H}^{reg}\mathbf{q} - \mathbf{g}\| + \lambda^2\|\mathbf{q} - \mathbf{q}_0\|$ using the L-curve method (see *TSVD with L-curve* above).
2. *Tikh. with GCV*: see *TSVD with GCV* above.
3. *Tikh. with QOC*: see *TSVD with QOC* above.
4. *Tikh. with Lagrange factor*: Minimization of the combined norm of $\|\mathbf{H}^{reg}\mathbf{q} - \mathbf{g}\| + \lambda^2\|\mathbf{q}\|$ is applied.

In the case of *Damped SVD (DSVD)*, we use the following methods:

1. *DSVD with LSQ optimized s-function*: Least square approximation of the solutions using a diagonal smoothing matrix $s_i = \exp((-i/a)^b)$, $i = 1, \dots, n$. Like in the case of the *TSVD LSQ optimized* above, we argue that the s-function parameters a and b are specific for a measurement problem and therefore are constant. That means a one-time estimation of a and b is sufficient and the estimation of the PSD with a predefined smoothing function is a very fast method.
2. *DSVD with L-curve*: see *TSVD with L-curve* above, but using a smoothing function.
3. *DSVD with GCV*: see *TSVD with GCV* above, but using a smoothing function.
4. *DSVD with QOC*: see *TSVD with QOC* above, but using a smoothing function.

For the Genetic Algorithm (GA), the Landweber-Bialy (L.-B.), the Chahine (Chah.) and the Inverse Monte Carlo (IMC) method we would like to refer to the references cited in table 1. However, we have slightly modified some algorithms. In the case of the IMC algorithm we implement a non-linear search algorithm. Each random PSD \mathbf{q}_i in an iteration is generated by an exponential form $\mathbf{q}_i = \mathbf{q}_0^X$ with an initial, randomly chosen distribution \mathbf{q}_0 and a random number $X \in [0, 6]$. This non-linearity accelerates the detection of solutions.

5 Results

In this section we will present some results we obtained from our simulations. They are presented in tables¹. Each row of the tables concern to one inversion method, described in Section 4. Because there are different methods within one inversion method (e.g. five different approaches of the Tikhonov regularization), we have marked the most exact result with a superscript corresponding to the related method in Section 4 (see row 'Tikh.' in Table 2). We simulate the scattering pattern of water droplets ($m = 1.33 + 0.0i$), illuminated by a plane wave ($\lambda = 514.5nm$). For a better comparability, all results are calculated by using the same number of $n_i = 24$ size classes.

Because of the stochastic nature of the added noise the quality of an inversion method may vary from run to run. Therefore, we have to perform several simulation runs for the same parameters but different noise. Of course, simulations with low noise probably should not generate differing results. This assumption was verified by repeating some

¹Additional results can be found in a supplementray file, see Section 8.

selected simulations. Only simulations with very noisy simulated measurements show occasionally a non-uniform convergence.

In all presented results we use a constant number of iterations for every iterative method. These are $n_{it} = 10^3, 10^5, 10^5$ and 10^6 for GA, L.-B., Chah. and IMC, respectively.

To test our implemented method, we first investigate the well known inverse problem of laser diffraction measurements, which are based on the measurement of the forward radiation [1]. We limit the scattering range to $0.5^\circ < \theta < 35^\circ$ in steps of a geometric series expansion resulting in 30 measured scattering ranges (e.g. [13]). The PSD is a log.-normal distribution (eq. (5)) with a mean diameter $\bar{d} = 2\mu\text{m}$ and a width parameter $\sigma = 0.4$, divided in $n_i = 24$ size classes. The results of this investigation are presented in Table 2. Each simulation result is represented by a block consisting of the four lines "problem", "LSQ difference" (Least Square difference), "modal value" and "computing time".

Method no.	SVD	TSVD	DSVD	NNLS	P.-T.	Tikh.	GA	L.-B.	Chah.	IMC
problem 1:	convergent measured scattering diagram; linear division of PSD									
LSQ difference:	3.54	3.54 ¹	6.51 ⁴	5.51	5.82 ²	6.19 ²	5.36	6.65	5.75	5.67
modal value: (μm)	2.68	2.68	3.11	2.68	2.68	3.11	9.14	2.68	2.68	2.68
computing time (s):	0.00	0.00	0.04	0.01	0.04	0.05	73.01	1661.55	1694.03	41.46
problem 2:	convergent measured scattering diagram; geometric series division of PSD									
LSQ difference:	9.52	4.27 ¹	5.89 ¹	6.49	7.09 ²	5.37 ²	6.25	7.20	6.51	7.04
modal value: (μm)	0.26	2.61	4.64	2.61	3.83	4.64	10.00	3.16	2.61	3.83
computing time (s):	0.00	0.00	0.36	0.01	0.03	0.04	73.51	446.37	175.19	41.93
problem 3:	randomly selected scattering diagrams; linear division of PSD									
LSQ difference:	3.53	3.07 ³	2.37 ³	3.48	2.62 ²	2.19 ³	5.36	2.54	2.48	2.75
modal value: (μm)	2.68	2.68	1.82	2.68	2.68	1.82	9.14	2.68	2.68	2.25
computing time (s):	0.01	0.03	0.03	0.00	0.04	0.03	73.27	6.04	17.06	42.21
problem 4:	randomly selected scattering diagrams; geometric series division of PSD									
LSQ difference:	9.87	3.52 ¹	3.50 ⁴	4.13	3.47 ²	3.68 ¹	6.25	3.77	3.98	4.98
modal value: (μm)	0.21	3.16	2.61	2.61	2.61	2.15	10.00	2.61	2.61	2.61
computing time (s):	0.01	0.00	0.03	0.01	0.04	0.16	66.00	1362.66	1289.63	41.59

Table 2: List of results; the footnotes in the respective row indicate different analysing methods which are described in section 4; a computing time of 0.00 means that it is lower than 10 ms; *fixed parameter*: log.-norm. PSD ($\bar{d} = 2\mu\text{m}$, width parameter $\sigma = 0.4$) in the size range of $0.1 \dots 10\mu\text{m}$, multiplicative noise with $p = 1\%$, unpolarized measured scattering diagrams; *varied parameter*: method to simulate the measurements and the kind of division of the PSD.

The results in Table 2 show that simulation of measurements using a limited number of particles according to the probability derived from the PSD leads to better results than convergent measurements. In addition, a linear division of the PSD delivers better results than a geometric series division. Besides their quickness, the truncated and the damped SVD yield the best result.

If we extend the measuring range to scattering angles of $5^\circ < \theta < 175^\circ$ and maintain the parameters above, the inversion algorithms have great problem to reproduce the given PSD². Then, an increase of the angular resolution up to $\Delta\theta = 0.5^\circ$, obtainable with high resolution CCD-cameras, leads to better results. This can be seen in Table 3 when comparing the results of problem 2 with the enhanced results of problem3. Furthermore, the increase of the number of nodes improves the quality of the results once more. However, the last observation is not relevant for measurements, but is import for simulations. Therefore, the measurement of a wide scattering range needs a very high angular resolution. This simulation result is in contrast with an analysis of the covariance matrix given by Twomey [9] which leads to the conclusion that such a high resolution results in very small eigenvalues without any physical meaning.

In the next simulation series we use particles with a PSD between $0.05 \dots 1\mu\text{m}$ and evaluate the full scattering range of $5^\circ < \theta < 175^\circ$. Additionally, we evaluate the measured light intensity twice under horizontal-horizontal (hh) as well as vertical-vertical (vv) polarization of this scattering range. This will be enabled by the capability of the ellipsoidal mirror to measure two opposite scattering diagrams (see Figure 1). The simulation results show better reproducibility of the given PSD with most of the inversion algorithms compared with the results in Table 2. To give an impression of the achieved simulation results Figure 5 shows two examples for algorithms which each yields the lowest least square difference. The left part is from Table 3 while the right part is from Table 4.

²Table 2 in the supplementary information.

Figure 5: Comparison of given (solid lines) and retrieved (dashed lines) PSDs in the size range of $0.05 \dots 1 \mu\text{m}$; (left) log.-normal PSD, best result of problem 8 of table 3: truncated SVD; (right) bimodal PSD, best result of problem 3 of table 4: the Chahine inversion method.

We explain the overswing behaviour by numerical instabilities. Oscillatory results are typical for inverse problems, and the inversion methods always show more or less instabilities, except that the noise level is very small.

We want to investigate now the effect of different kinds of noise for small particles. Table 3 lists results of simulations using either additive or multiplicative noise.

Method no.	SVD	TSVD	DSVD	NNLS	P-F.	Tikh.	GA	L-B.	Chah.	IMC
problem 1:	unpolarized, $\Delta\theta = 1^\circ$, noise: addit. with SNR = 20dB									
LSQ difference:	5.79	1.66 ²	5.74 ²	5.74	6.13 ¹	1.09 ²	3.56	2.38	3.01	6.58
modal value (μm):	0.05	0.42	0.46	0.05	0.05	0.38	0.34	0.46	0.34	0.13
computing time (s):	0.01	0.06	0.08	0.02	0.01	0.05	360.92	29.76	22.23	52.88
problem 2:	unpolarized, $\Delta\theta = 1^\circ$, noise: addit. with SNR = 30dB									
LSQ difference:	5.78	1.77 ¹	6.13 ²	3.67	4.70 ²	1.81 ¹	2.09	2.64	1.97	4.79
modal value (μm):	0.05	0.38	0.42	0.30	0.50	0.42	0.38	0.50	0.38	0.13
computing time (s):	0.01	0.00	0.07	0.02	0.04	0.20	369.81	44.92	22.09	53.91
problem 3:	unpolarized, $\Delta\theta = 0.5^\circ$, noise: addit. with SNR = 30dB									
LSQ difference:	5.79	1.18 ¹	4.54 ¹	2.53	2.98 ²	1.27 ¹	1.99	2.49	0.98	4.79
modal value (μm):	0.05	0.38	0.50	0.34	0.34	0.38	0.34	0.46	0.34	0.13
computing time (s):	0.01	0.00	0.04	0.04	0.05	0.22	724.89	42.10	25.63	66.19
problem 4:	hh + vv polarization, $\Delta\theta = 0.5^\circ$, noise: addit. with SNR = 30dB									
LSQ difference:	5.85	0.81¹	3.99 ¹	2.78	4.66 ²	3.23 ¹	0.88	2.40	2.83	4.68
modal value (μm):	0.05	0.38	0.38	0.34	0.30	0.38	0.38	0.46	0.38	0.34
computing time (s):	0.00	0.00	0.02	0.04	0.04	0.17	1442.67	55.87	31.40	89.25
problem 5:	unpolarized, $\Delta\theta = 0.5^\circ$, noise: multiplicative with noise factor $p = 10\%$									
LSQ difference:	5.77	0.96 ¹	3.49 ²	2.15	7.73 ¹	0.94 ²	1.58	2.49	0.34	3.15
modal value (μm):	0.05	0.38	0.34	0.34	0.09	0.38	0.34	0.46	0.38	0.46
computing time (s):	0.01	0.00	0.15	0.06	0.00	0.14	719.14	39.85	24.80	65.50
problem 6:	hh + vv polarization, $\Delta\theta = 0.5^\circ$, noise: multiplicative with noise factor $p = 10\%$									
LSQ difference:	5.86	3.51 ¹	6.42 ¹	5.76	3.80 ²	6.08 ¹	1.22	2.42	5.75	3.95
modal value (μm):	0.05	0.38	0.38	0.05	0.34	0.38	0.38	0.46	0.05	0.46
computing time (s):	0.00	0.00	0.39	0.03	0.04	0.20	1441.67	57.86	31.24	89.13
problem 7:	unpolarized, $\Delta\theta = 0.5^\circ$, noise: multiplicative with noise factor $p = 1\%$									
LSQ difference:	5.77	0.77 ¹	2.69 ¹	3.37	3.87 ²	0.80 ²	1.77	2.49	0.10	3.10
modal value (μm):	0.05	0.38	0.38	0.38	0.46	0.38	0.46	0.46	0.38	0.42
computing time (s):	0.02	0.00	0.36	0.04	0.08	0.04	719.89	48.33	24.91	65.64
problem 8:	hh + vv polarization, $\Delta\theta = 0.5^\circ$, noise: multiplicative with noise factor $p = 1\%$									
LSQ difference:	5.86	0.93¹	1.11 ¹	5.68	3.37 ²	1.55 ¹	1.66	2.38	5.27	3.95
modal value (μm):	0.05	0.38	0.38	0.09	0.38	0.38	0.38	0.46	0.09	0.46
computing time (s):	0.01	0.01	0.05	0.06	0.09	0.13	1284.44	91.33	43.43	70.84

Table 3: Fixed parameters: log.-norm. PSD from $0.05 \dots 1 \mu\text{m}$ with modal value $d_{mod} = 0.38 \mu\text{m}$ and $d_{10} = 0.31 \mu\text{m}$ and $d_{90} = 0.52 \mu\text{m}$, size classes: 24, scat. range: $\theta = 5 - 175^\circ$; varied parameters: scattering resolution, the kind of noise and the value of the noise.

In case of additive noise (first 4 simulations presented in Table 3), it can be observed that a higher angular resolution (from $\Delta\theta = 1^\circ$ to $\Delta\theta = 0.5^\circ$) yields better results. A decrease in noise by increasing the SNR will in general not necessarily improve the quality of the results. For instance, the Tikhonov regularization algorithms, where one of them yields the best result in problem 1, get worse results in the case of less noise in problem 2. Altogether, it is not possible to define a general rule or to observe unambiguous tendencies for the

performance of the individual inversion methods. In the case of multiplicative noise (last 4 simulations), most of the inversion methods perform better at lower noise level. At a noise level of 10%, the genetic algorithm method yields the lowest least square difference, but also the longest computing time. It can be seen that the computing time of the GA increase linearly with an increase of the angular resolution, while the other iterative methods (L-B., Chah., IMC) show a slower increase. When using the hh- and the vv-polarization simultaneously, the computing time of GA exceeds 20 minutes.

In Table 4, we now compare the results of the inversion methods when additive and multiplicative noise are applied simultaneously to the simulated measurements. Therefore, each intensity $I_n(\theta, \lambda, m(\lambda), x)$ (eqn.(1)) will be disturbed by multiplicative noise with $p = 0.1\%$. After the integration (i.e. the resulting $I(\theta, \lambda)$ from eqn.(1)) we apply additive noise with a $SNR = 30dB$. Additionally, we compare the performance of the inversion methods for two log.-normal PSDs with the same mean diameter but different widths and for a bimodal PSD.

Method no.	SVD	TSVD	DSVD	NNLS	P-T.	Tikh.	GA	L-B.	Chah.	IMC
problem 1:	$\bar{d} = 0.4\mu m, \sigma = 0.2, \bar{d}_{mod} = 0.38\mu m, d_{10} = 0.31\mu m, d_{90} = 0.52\mu m, \text{unpol.}$									
LSQ difference:	5.81	1.24 ⁴	4.86 ²	3.05	4.55 ²	1.20 ¹	5.76	2.51	0.17	4.80
modal value: (μm)	0.05	0.42	0.42	0.34	0.30	0.42	0.96	0.46	0.38	0.13
computing time (s):	0.00	0.02	0.07	0.02	0.05	0.17	796.94	92.39	23.66	64.99
problem 2:	$\bar{d} = 0.4\mu m, \sigma = 0.4, \bar{d}_{mod} = 0.32\mu m, d_{10} = 0.22\mu m, d_{90} = 0.61\mu m, \text{unpol.}$									
LSQ difference:	24.87	16.34 ³	17.43 ²	25.07	22.30 ¹	17.97 ¹	24.95	17.04	17.66	21.95
modal value: (μm)	0.05	0.05	0.13	0.05	0.13	0.38	0.96	0.50	0.34	0.34
computing time (s):	0.00	0.07	0.08	0.04	0.01	0.18	803.65	126.48	23.93	65.08
problem 3:	bimodal distr.: $\bar{d}_{mod_1} = 0.22, \bar{d}_{mod_2} = 0.62\mu m, \text{unpol.}$									
LSQ difference:	7.17	3.55 ⁵	7.14 ²	7.18	6.41 ¹	5.18 ²	7.18	5.25	1.37	5.09
modal value: (μm)	0.05	0.63	0.05	0.05	0.09	0.63	0.96	0.63	0.21	0.63
computing time (s):	0.00	0.07	0.08	0.03	0.01	0.04	805.27	114.71	23.56	65.76
problem 4:	$\bar{d} = 0.4\mu m, \sigma = 0.2, \bar{d}_{mod} = 0.38\mu m, d_{10} = 0.31\mu m, d_{90} = 0.52\mu m, \text{hh + vv polarization}$									
LSQ difference:	5.86	1.06 ²	5.04 ²	2.96	5.93 ¹	3.38 ¹	5.76	2.40	0.41	3.93
modal value: (μm)	0.05	0.42	0.38	0.38	0.05	0.38	0.96	0.46	0.38	0.38
computing time (s):	0.01	0.08	0.08	0.04	0.00	0.18	1615.00	130.19	57.21	89.58
problem 5:	$\bar{d} = 0.4\mu m, \sigma = 0.4, \bar{d}_{mod} = 0.32\mu m, d_{10} = 0.22\mu m, d_{90} = 0.61\mu m, \text{hh + vv polarization}$									
LSQ difference:	9.38	3.58 ¹	6.07 ¹	5.21	6.39 ²	3.93 ¹	9.29	5.78	0.72	5.97
modal value: (μm)	0.05	0.38	0.46	0.42	0.34	0.42	0.96	0.50	0.38	0.34
computing time (s):	0.00	0.00	0.01	0.05	0.11	0.17	1601.97	101.93	51.11	89.66
problem 6:	bimodal distr.: $\bar{d}_{mod_1} = 0.22, \bar{d}_{mod_2} = 0.62\mu m, \text{hh + vv polarization}$									
LSQ difference:	7.23	4.83 ¹	6.41 ²	3.89	4.06 ²	5.06 ¹	7.18	5.03	2.14	4.58
modal value: (μm)	0.05	0.63	0.63	0.21	0.63	0.63	0.96	0.63	0.21	0.59
computing time (s):	0.01	0.00	0.09	0.03	0.11	0.20	1605.94	108.27	47.91	89.02

Table 4: *Fixed parameters:* the PSDs are between $0.05 \dots 1\mu m$, the scattering range is $\theta = 5^\circ \dots 175^\circ$ with $\Delta\theta = 0.5^\circ$, there is no scaling of the scattering diagrams, and the value of the multiplicative noise is 0.1% and that of the additive noise is $SNR = 30dB$; *varied parameters:* three different PSDs (two different log.-norm. PSDs (both with an arithmetic mean diameter $\bar{d} = 0.4\mu m$ but $\sigma = 0.2$ and a broader PSD with $\sigma = 0.4$) and one bimodal log.-norm. PSD (two added log.-norm. PSDs with $\bar{d}_1 = 0.22\mu m, \sigma_1 = 0.25$ and $\bar{d}_2 = 0.62\mu m, \sigma_2 = 0.08$)) and different polarizations.

The results presented are different from those in the other tables by the fact that we here apply both kinds of noise. The simulated measurements calculated in this way can be considered as very noisy.

The results in Table 4 shows again that the increase of the number of measurements may be able to enhance the quality of the data retrieval although the information content of the eigenvalues, discussed at the end of Section 3.2, is very small. In problem 2, no inversion method retrieve the broad PSD, while in problem 5 – the same PSD but measuring hh as well as vv polarization – the Chahine method retrieves the reasonably well.

6 Conclusion

In this paper we investigate simulation of scattering measurements of spherical particles and the usefulness of inversion methods on different measurement setups and size distributions. A necessary condition for testing different inversion methods is a correct generation of realistic measurement data. Another important modeling parameter for the simulation of measurements is the number of nodes used by the integration of the measured scattering data. Measured data are usually disturbed, but often the background for the interferences are not exactly known. Therefore, the stochastic concept of noise is used in this paper,

i.e. noise is applied to the simulated data and the behaviour of the inversion methods to different kinds and levels of noise are investigated.

The other varied parameters are related to measurement setups. For instance the measurement resolution of the scattering angles is important to retrieve the particle size distribution. In the case of the measurement of a wide range of angles we notice that larger particles require a higher angular resolution.

Our focus of interest is to find out which inversion method is ideal when using a measurement setup with an elliptical mirror. The answer depends on the assumed particle sizes. The best results are frequently provided by the iterative methods. In particular, the Chahine iteration method, which is additionally the fastest of them, yields frequently the best results for a simulation³. The Landweber-Bialy algorithm delivers good results as well in the case of large particles and extended scattering range.

If we consider inversion methods with regularization, the L-curve method seems to be a very suitable criterion to find a correct solution, especially in comparison with GCV (e.g. TSVD and DSVD, method 3). This was also stated by Kandlikar and Ramachandran [6].

The fastest and additionally one of the most stable inversion algorithm investigated in this work is the truncated singular value decomposition (TSVD). It may be used in measuring applications where on-line evaluation is required.

The shown results (especially that from Table 2) confirm that in the case of laser diffraction measurements the Phillips-Twomey inversion method is a good approach.

In general, because no inversion method yields satisfactory results for all investigated cases, even not for one specific measurement setup, we recommend to investigate simulations of the particular problem considering several inversion methods and variation of different parameters.

7 Acknowledgment

The authors acknowledge the support of this research project by the Deutsche Forschungsgemeinschaft (DFG).

8 Supporting Information

We have put together some additional simulation results presented in tables. This material is available as supplementary information free of charge via the Internet at <http://www3.interscience.wiley.com/jou>

³In case of very noisy measurement conditions, the genetic algorithm approach yields the best results; see the supplementary file.

9 Symbols and Abbreviations

Ca	capillary number
\bar{d}	mean droplet diameter
d_{50}	median value
d_{mod}	modal value
d_{xx}	xx-quantile value
D	droplet deformation
$g(\theta)$	measured value/intensity
\mathbf{H}	kernel matrix
$h(\theta, x)$	element of \mathbf{H}
$I(\theta)$	intensity scattered at angle θ
$m(\lambda)$	refractive index of the particles
n_i	number of size classes
n_{mode}	number of nodes for the integral estimation
N	number of particles within a scattering volume
$q(x)$	number of particles with diameter x (PSD)
$\Delta\mathbf{Q}$	frequency distribution
v	droplet velocity
x	number of particles within a scattering volume
ϵ	additive noise
γ	multiplicative noise
κ	condition number of \mathbf{H}
λ	wavelength
θ	scattering angle
N	number of particles within a scattering volume
Chah.	Chahine iteration
DSVD	Damped SVD
GA	Genetic Algorithm
GCV	Generalized Cross Validation
hh	horizontal-horizontal measured intensity
IMC	Inverse Monte-Carlo
L.-B.	Landweber-Bialy iteration
NNLS	Non-Negative Least Squares
PSD	Particle Size Distribution
P.-T.	Phillips-Twomey regularization
QOC	Quasi Optimality Criterion
SNR	Signal-to-Noise Ratio
SVD	Singular Value Decomposition
Tikh.	Tikhonov regularization
TSVD	Truncated SVD
unpol.	unpolarised measured intensity
vv	vertical-vertical measured intensity

10 References

References

- [1] R. Xu. *Particle Characterization: Light Scattering Methods*. Kluwer Academic Publishers, 2000.
- [2] P. C. Hansen. *Rank-deficient and discrete ill-posed problems: numerical aspects of linear inversion*. SIAM, Philadelphia, 1998.
- [3] A. G. Ramm. *Inverse Problems. Mathematical and Analytical Techniques with Application to Engineering*. Springer, Boston, 2005.
- [4] A. Tarantola. *Inverse Problem Theory and Methods for Model Parameter Estimation*. SIAM, Philadelphia, 2005.

- [5] D. N. Ghosh Roy and L. S. Couchman. *Inverse Problems and Inverse Scattering of Plane Waves*. Academic Press, 2002.
- [6] M. Kandlikar and G. Ramachandran. Inverse methods for analysing aerosol spectrometer measurements: A critical review. *J. Aerosol Sci.*, 30:413–437, 1999.
- [7] J. Vargas-Ubera, J. F. Aguilar, and D. M. Gale. Reconstruction of particle-size distributions from light-scattering patterns using three inversion methods. *Appl. Opt.*, 46:124–132, 2007.
- [8] J. H. Koo and E. Dan Hirleman. Synthesis of integral transform solutions for the reconstruction of particle-size distributions from forward-scattered light. *Appl. Opt.*, 31:2130–2140, 1992.
- [9] S. Twomey. *Introduction to the mathematics of inversion in remote sensing and indirect measurements*. Elsevier, New York, 1977.
- [10] L. P. Bayvel, J. Knight, and G. Robertson. Alternative model-independent inversion programme for malvern particle sizer. *Part. Charact.*, 4:49–53, 1987.
- [11] L. P. Bayvel, P. Eisenklam, M. Symons, and R. Wood. An instrument for particules size distribution measurements in the submicronic size range. *Atomis. Spray Techn.*, 3:135–143, 1987.
- [12] L. C. Chow and C. L. Tien. Inversion techniques for determining the droplet size distribution in clouds: numerical examination. *Appl. Opt.*, 15:378–383, 1976.
- [13] M. Heuer and K. Leschonski. Results obtained with a new instrument for the measurement of particle size distributions from diffraction patterns. *Part. Charact.*, 2:7–13, 1985.
- [14] R. Weichert and H. Mühlenweg. Development of a new optical particle sizer for the measurement of wide particle size distributions in hot gases. In J. Schwedes, editor, *Fine Solid Particles.*, pages 318–325. Shaker, 1997.
- [15] H. Schnablegger and O. Glatter. Optical sizing of small colloidal particles: an optimized regularization technique. *Appl. Opt.*, 30:4889–4896, 1991.
- [16] Z. Sun and E. M. Sevick-Muraca. Inversion algorithms for particle sizing with photon migration measurement. *AIChEJ*, 47:1487–1498, 2001.
- [17] M. T. Chahine. Inverse problems in radiative transfer: Determination of atmospheric parameters. *J. Atmosph. Sci*, 27:960–967, 1970.
- [18] F. Ferri, M. Giglio, and U. Perini. Inversion of light scattering data from fractals by the chahine iterative algorithm. *Appl. Opt.*, 28:3074–3082, 1989.
- [19] M. Mitschke. *PDA-relevante Streulichteigenschaften: Phänomene, Parameterwahl und mathematische Korrektur*. VDI Verlag, 2000.
- [20] L. Landweber. An iteration formula for fredholm integral equations of the first kind. *Am. J. Math.*, 73:615–624, 1951.
- [21] W. Q. Yang, D. M. Spink, and H. McCann. An image-reconstruction algorithm based on landweber’s iteration method for electrical-capacitance tomography. *Meas. Sci. Technol.*, 10:1065–1089, 1999.
- [22] R. J. W. Hodgson. Genetic algorithm approach to particle identification by light scattering. *J. Coll. Interf. Sci.*, 229:399–406, 2000.
- [23] B. Barkey, S. E. Paulson, and A. Chung. Genetic algorithm inversion of dual polarization polar nephelometer data to determine aerosol refractive index. *Aerosol Sci. Technol.*, 41:751–760, 2007.
- [24] C. A. O. Nascimento, R. Guardani, and M. Giulietti. Use of neural networks in the analysis of particle size distributions by laser diffraction. *Powder Technol.*, 90:89–94, 1997.

- [25] Z. Wang, Z. Ulanowski, and P. H. Kaye. On solving the inverse scattering problem with rbf neural networks: Noise-free case. *Neural Comput. and Applic.*, 8:177–186, 1998.
- [26] P. Coppens, L. Deriemaeker, and R. Finsy. Shape and size determination by laser diffraction: Feasibility of data analysis by neural networks. *Part. Part. Syst. Charact.*, 17:117–125, 2000.
- [27] C. S. Hodges, J. A. S. Cleaver, M. Ghadiri, R. Jones, and H. M. Pollock. Forces between polystyrene particles in water using the afm: Pull-off force vs particle size. *Langmuir*, 18:5741–5748, 2002.
- [28] M. Ye, S. Wang, Y. Lu, T. Hu, Z. Zhu, and Y. Xu. Inversion of particle-size distribution from angular light-scattering data with genetic algorithms. *Appl. Opt.*, 38:2677–2685, 1999.
- [29] D. A. Ligon, T. W. Chen, and J. B. Gillespie. Determination of aerosol parameters from light-scattering data using an inverse monte carlo technique. *Appl. Opt.*, 35:4297–4303, 1996.
- [30] S. D. Coston and N. George. Particle sizing by inversion of the optical transform pattern. *Appl. Opt.*, 30:4785–4794, 1992.
- [31] S. K. Friedlander. *Smoke, Dust, and Haze. Fundamentals fo Aerosol Dynamics*. Oxford University Press, 2000.
- [32] K. B. Aptowicz and R. K. Chang. Angularly-resolved elastic scatter from single particles collected over a large solid angle and with high resolution. *J. Phys.: Conf. Series*, 6:90–96, 2005.
- [33] S. Arridge, P. van der Zee, D. T. Delpy, and M. Cope. Particles sizing in the Mie scattering region: singular-value analysis. *Inv. Prob.*, 5:671–689, 1989.
- [34] H. A. Stone. Dynamics of drop deformation and breakup in viscous fluids. *Annu. Rev. Fluid Mech.*, 26:65–102, 1994.
- [35] C. Crowe, M. Sommerfeld, and Y. Tsuji. *Multiphase flows with droplets and particles*. CRC Press, Boca Raton, 1998.
- [36] A. H. Lefebvre. *Atomization and Sprays*. Hemisphere Publishing Corporation, New York, 1989.
- [37] K. Hedrih and V. Babovic and D. Sarkovic. An auxiliary size distribution model for the ultrasonically produced water droplets. *Experim. Therm. Fluid Sci.*, 30:559–564, 2006.
- [38] C. Bohren and D. Huffman. *Absorption and Scattering of Light by Small Particles*. Wiley and Sons, New York, 1983.
- [39] A. A. Kokhanovsky. *Optics of Light Scattering Media*. Springer, Chichester, 2001.
- [40] W. Wiscombe. Improved mie scattering algorithm. *Appl. Opt.*, 19:1505–1509, 1990.
- [41] N. C. Ford. Light scattering apparatus. In R. Pecora, editor, *Dynamic Light Scattering. Applications of Photon Correlation Spectroscopy*. Plenum Press, 1985.
- [42] A. C. Bovik. On detecting edges in speckle imagery. *IEEE Trans. Acoust. Speech Signal Process.*, 36:1618–1627, 1988.
- [43] P. A. Kelly, H. Derin, and K. D. Hartt. Adaptive segmentation of speckled images using a hierarchical random field model. *IEEE Trans. Acoust. Speech Signal Process.*, 36:1628–1641, 1988.
- [44] R.J. Mammone and X. Zhang. Robust speech processing as an inverse problem. In V. K. Madisetti and D. B. Williams, editors, *Digital Signal Processing Handbook*. CRC Press, Boca Raton, 1999.
- [45] G. B. Giannakis. Cyclostationary signal analysis. In V. K. Madisetti and D. B. Williams, editors, *Digital Signal Processing Handbook*. CRC Press, 1999.

- [46] B. P. Lathi. *Modern Digital and Analog Communication Systems*. Oxford University Press, New York, 1998.
- [47] J. He, S.-M. Wang, J.-C. Cheng, and S.-Y. Zhang. Inversion of particle size distribution from light scattering spectrum. *Inv. Probl.*, 12:633–639, 1996.
- [48] M. Ye, S. Wang, and Y. Xu. An inverse technique devised from modification of annealing-evolution algorithm for particle sizing by light scattering. *Powd. Techn.*, 104:80–83, 1999.
- [49] K. D. Kammeyer and K. Kroschel. *Digitale Signalverarbeitung. Filterung und Spektralanalyse mit MATLAB-Übungen*. Teubner, Stuttgart, 2004.
- [50] C. L. Lawson and R.J. Hanson. *Solving Least Squares Problems*. Prentice Hall, Englewood Cliffs, 1974.